drones

MDPI

Article

Globally Attractive Hyperbolic Control for the Robust Flight of an Actively Tilting Quadrotor

Santos Miguel Orozco Soto [1,*], Fabio Ruggiero [1,2] and Vincenzo Lippiello [1,2]

[1] Consorzio C.R.E.A.T.E., Via Claudio 21, 80125 Naples, Italy
[2] Department of Electrical Engineering and Information Technology, University of Naples Federico II, Via Claudio 21, 80125 Naples, Italy
* Correspondence: sorozco@ctrl.cinvestav.mx

Abstract: This paper addresses the problem of robustly controlling an actively tilting quadrotor UAV. The proposed technique is model-free and it is based on hyperbolic functions of the six-dimensional pose error of the UAV with respect to the world reference frame; this hyperbolic controller globally attracts the error signals to an ultimate bound about the origin despite external disturbances, which is proved by way of a strict Lyapunov function based analysis. The effectiveness of the controller is evaluated by means of tracking and regulation experiments on adverse conditions, which were implemented on a virtual model of the UAV through a physics-engine-based simulation environment that provides an almost identical behaviour than a real UAV. The norm of the six-dimensional error signal converged to zero for the regulation experiments, whereas for tracking it did not exceed 0.05 meters, which indicated a successful operation of the control system. In addition, the performance of the hyperbolic controller was contrasted against a nonlinear PID, which resulted in a better performance in favour of the first one, who settled the errors to zero up to eight seconds before and demanded up to 2000 less revolutions per minute from the rotors while performing the same regulation tasks. All the aforesaid successful results place the proposed technique as a competitive alternative for controlling actively tilting multirotors due to its simplicity, robustness and demonstrated effectiveness.

Keywords: hyperbolic control; UAV control; actively tilting quadrotor; omnidirectional UAV

Citation: Orozco Soto, S.M.; Ruggiero F.; Lippiello, V. Globally Attractive Hyperbolic Control for the Robust Flight of an Actively Tilting Quadrotor. *Drones* **2022**, *6*, 373. https://doi.org/10.3390/drones6120373

Academic Editor: Andrey V. Savkin

Received: 2 November 2022
Accepted: 20 November 2022
Published: 23 November 2022

1. Introduction

Tilting multirotor unmanned aerial vehicles (UAV) are capable of executing six degree-of-freedom (DOF) motions due to the vectored thrust supplied by its propellers. This class of UAV has become an advantageous tool in a huge variety of applications that require overcoming the underactuation property of common non tiling multirotor UAVs; the choice of the number of rotors and their passively (fixed) or actively (moving) property depend on the requirements of the application [1]. Despite the advantages of passively tilted multirotors regarding their simplicity from a mechanical and control systems point of view [1], actively tilting the propellers provides more versatility and it is also more useful for controlled force delivery (interaction) tasks [2]. In light of this, controlling actively tilting multirotors is not a trivial task due to several factors: first of all, they are highly nonlinear systems as other types of UAV, and in some cases, it is difficult to obtain accurate dynamic models that are useful for developing an effective control strategy. Secondly, disturbances might affect an actively tilting multirotor while flying whether in outdoors or indoors scenarios. Finally, mapping the computed six-dimensional controller to the desired rotor speeds and propeller's orientation can represent a challenge depending on the number of rotors that the UAV is equipped with.

In this regard, this paper addresses the problem of effectively and robustly controlling an actively tilting quadrotor UAV through a control technique that is common for other

types of robotic systems but is novel within the field of UAVs [3]. The organization of the manuscript is as follows: the present section continues with a review of the literature about the control of actively tilting quadrotors, as well as the problem statement, the proposed solution and the contributions of the work. Section 2 describes some mathematical definitions and preliminaries that are useful for the controlled system analysis. Section 3 details the actively tilted quadrotor dynamics and its properties. Section 4 explains the control system proposal as well as its stability and allocation to the UAV actuation system. The assessment of the controller through physics-engine-based simulations on a virtual UAV are presented in Section 5. Section 6 concludes the manuscript.

1.1. Literature Review about Control of Actively Tilting Quadrotors

The problem of regulation and tracking for actively tilting quadrotors has been of interest for the last decade. Some authors have obtained convenient simulation results through model-based controllers, namely, feedback-linearisation-based and differential flatness techniques [4–6]. Additionally, some researchers have successfully implemented model-based controllers in real, actively tilting quadrotors, as is presented in [7–9]. These aforementioned controllers require an accurate knowledge of the dynamic model of the system to work properly. Moreover, the precision of the regulation or tracking tasks might be compromised by external disturbances or by unconsidered dynamics, awakening the necessity of applying other types of control strategies that could deal with the aforesaid difficulties.

In contrast, several examples of regulation and tracking controllers for actively tilting quadrotors are available in the literature. For instance, H_∞ control, active disturbance rejection control (ADRC) and adaptive neural control have been applied by some researchers, showing successful numerical simulation results [10–12]; the two first works do not contain either the stability proof of the closed-loop system, nor the allocation of the controller to the tilting angles and angular velocities of the propellers, which is also missing in [12].

Alternatively, sliding mode control (SMC)-related techniques have received particular attention by the community. The works in [13] and in [10] presented feedback linearization schemes adding a discontinuous term to the controller; nonetheless, the stability was not clearly proved in either paper and the allocation of the controller was not described either. A recent work that used the sliding mode technique only for the translational motion degrees-of-freedom (DOFs) of the tilting quadrotor was reported in [14]. Despite the favourable numerical simulations obtained, the implementation of all these forenamed tactics is arguable, since the discontinuous control signal demands a high-frequency switching (*chattering* effect) of the propellers' angles. From the electromechanical point of view, performing discontinuous control signals is likely unfeasible and potentially dangerous for the tilting mechanisms of the propellers and for the power drivers as well.

As an effort to reduce the *chattering* effect, some authors proposed the use of second-order SMC [12,15]. Although the theoretical and numerical results of these works are promising, they are only valid for six-DOF rigid bodies rather than tilting quadrotors, as a consequence of neglecting the allocation of the controller.

A recent contribution, presented in [16], showed satisfactory simulation results about the control of a tilting quadrotor; the authors proposed the use of a model-based controller enhanced with an extended-state observer to estimate and compensate for the external disturbances. Certainly, the observer increased the tuning parameters of the overall control system.

1.2. Problem Statement and Proposed Solution

Considering the cited literature, there are still some opportunity areas to improve the robust control of actively tilting quadrotors. For instance, a robust-enough controller but effortless and feasible to implement would be appropriate for actively tilted quadrotors developed from scratch. Moreover, a huge gap is yet present between the simulation and the implementation of control systems for UAVs; to the best of the authors' knowledge, the implementation of a robust control on a virtual or an actual tilting quadrotor has not

been reported so far. Against this background, this work presents the implementation of a model-free controller for robust regulation and tracking of a quadrotor with tilting propellers. This control scheme exploits the hyperbolic functions of the six-dimensional position error and its integral, which is helpful to deal with several kinds of disturbances. The global attractiveness to an ultimate bound about the origin of the error signals is demonstrated by means of a strict Lyapunov function based analysis.

The effectiveness of the proposed hyperbolic controller was assessed by means of four different study cases: (i) tracking a trajectory, (ii) commanding large-step-shaped set points, (iii) applying external wrenches caused by the motion of a robotic board mounted on the UAV and (iv) comparing the hyperbolic control against a state-of-the-art technique. All the experiments were carried out on a virtual quadrotor within a physics-engine-based simulation environment, which provides performance almost identical to real experiments; this is possible in virtue of the several physical phenomena that the simulator takes into account by default.

1.3. Contributions of the Work

The contributions of this work to the state of the art are the following:

- The proposed hyperbolic control is inspired by some related works that have been successfully applied to other types of robotic systems [3]. To the best of the authors' knowledge, this is the first time that a hyperbolic controller has been applied to the field of UAVs.
- Different from some texts, this paper presents a theoretically sound controller. Moreover, the allocation technique is included, which places this paper within a reduced set of published manuscripts that include both aspects.
- To the best of the authors' knowledge, this is the first time that a robust model-free controller is implemented in an actively tilting quadrotor whose behaviour is almost identical to an actual UAV, which is possible due to the utilization of a physics-engine-based simulation approach.

2. Mathematical Preliminaries

This section contains some mathematical definitions and properties that are useful later in the manuscript, to analyse the behaviour of the solutions of the differential equations representing the closed-loop system compound by the actively tilting quadrotor dynamics and the proposed controller. Thus, some properties of the used functions in the controller are briefly described below.

Beginning with the definitions, consider a matrix $\mathbf{H} \in \mathbb{R}^{n \times n}$, whose spectral norm is denoted along the manuscript as $\|\mathbf{H}\|$ and is given by

$$\|\mathbf{H}\| = \sqrt{\lambda_{\max}\{\mathbf{H}^T\mathbf{H}\}}, \tag{1}$$

where $\lambda_{\max}\{\cdot\}$ denotes the maximum or largest eigenvalue. For the case of symmetric matrices, the spectral norm can also be obtained by $\|\mathbf{H}\| = \lambda_{\max}\{\mathbf{H}\}$. Consider also a generic vector $\mathbf{x} \in \mathbb{R}^n$; hereafter in the text, the norm of any vector is defined as $\|\mathbf{x}\| \triangleq \sqrt{x_1^2 + x_2^2 + \cdots + x_n^2}$. Now, let $\mathbf{y}$ be an n-dimensional real-valued vector and let $\mathbf{tanh}(\mathbf{x}) : \mathbb{R}^n \to \mathbb{R}^n$ be a vector function such that

$$\mathbf{tanh}(\mathbf{x}) \triangleq \begin{bmatrix} \tanh(x_1) & \tanh(x_2) & \cdots & \tanh(x_n) \end{bmatrix}^T. \tag{2}$$

The norm $\|\mathbf{tanh}(\mathbf{x})\|$ satisfies the following

$$\|\mathbf{tanh}(\mathbf{x})\| = \sqrt{\sum_{i=1}^{n} \tanh^2(x_i)} \leq \sqrt{\sum_{i=1}^{n} 1_1^2 + 1_2^2 + \cdots + 1_n^2} = \sqrt{n}, \tag{3}$$

$$\|\mathbf{tanh}(\mathbf{x})\| \leq \|\mathbf{x}\|, \tag{4}$$

$$\mathbf{y}^T \mathbf{H} \mathbf{tanh}(\mathbf{x}) \leq \|\mathbf{y}\| \|\mathbf{H}\| \sqrt{n} \leq \|\mathbf{y}\| \|\mathbf{H}\| \|\mathbf{x}\|. \tag{5}$$

Notice that both Equations (3) and (4) are upper bounds of $\|\mathbf{tanh}(\mathbf{x})\|$; therefore, either can be chosen for the best mathematical convenience. Let as well $\boldsymbol{\varsigma}(\mathbf{x}) : \mathbb{R}^6 \to \mathbb{R}^6$ be a vector function given by

$$\boldsymbol{\varsigma}(\mathbf{x}) \triangleq \begin{bmatrix} \sqrt{\ln(\cosh(x_1))} & \sqrt{\ln(\cosh(x_2))} & \cdots \sqrt{\ln(\cosh(x_n))} \end{bmatrix}^T. \tag{6}$$

The time derivative of $\boldsymbol{\varsigma}(\mathbf{x})$ can be expressed as

$$\dot{\boldsymbol{\varsigma}}(\mathbf{x}) \triangleq \operatorname{diag}\left(\frac{\tanh(x_1)}{2\sqrt{\ln(\cosh(x_1))}}, \ \cdots, \ \frac{\tanh(x_n)}{2\sqrt{\ln(\cosh(x_n))}} \right) \dot{\mathbf{x}}. \tag{7}$$

It can be observed that $\dot{\boldsymbol{\varsigma}}(\mathbf{x})$ can be decomposed in the following ways

$$\dot{\boldsymbol{\varsigma}}(\mathbf{x}) = \begin{bmatrix} \tanh(x_1) \\ \vdots \\ \tanh(x_n) \end{bmatrix}^T \operatorname{diag}\left(\frac{1}{2\sqrt{\ln(\cosh(x_1))}}, \ \cdots, \ \frac{1}{2\sqrt{\ln(\cosh(x_n))}} \right) \dot{\mathbf{x}} \tag{8}$$

$$\text{or } \dot{\boldsymbol{\varsigma}}(\mathbf{x}) = \begin{bmatrix} \frac{1}{2\sqrt{\ln(\cosh(x_1))}} \\ \frac{1}{2\sqrt{\ln(\cosh(x_n))}} \end{bmatrix}^T \operatorname{diag}(\tanh(x_1), \ \cdots, \ \tanh(x_n)) \dot{\mathbf{x}} \tag{9}$$

3. Dynamics of Actively Tilting Quadrotor

Consider the Figure 1, where the world, airframe and propellers reference frames are presented. Then, the position and orientation of the UAV with respect to the world frame can be expressed as $\mathbf{p}_b \in \mathbb{R}^3 \triangleq \begin{bmatrix} {}^W x_b & {}^W y_b & {}^W z_b \end{bmatrix}^T$ and $\boldsymbol{\eta}_b = \begin{bmatrix} \phi & \theta & \psi \end{bmatrix}^T$, respectively where $\boldsymbol{\eta}_b$ is the orientation formed by the Euler angles *roll, pitch* and *yaw*. Thus, the six-dimensional pose is given by

$$\boldsymbol{\xi} \in \mathbb{R}^6 = \begin{bmatrix} \mathbf{p}_b^T & \boldsymbol{\eta}_b^T \end{bmatrix}^T. \tag{10}$$

Using the Newton–Euler formulation and after some algebra, the dynamics of the actively tilting quadrotor can be written as

$$\mathbf{D}(\boldsymbol{\xi}) \ddot{\boldsymbol{\xi}} + \mathbf{C}(\boldsymbol{\xi}, \dot{\boldsymbol{\xi}}) \dot{\boldsymbol{\xi}} + \mathbf{g} + \mathbf{w}_e(\cdot) = \boldsymbol{\Gamma}(\boldsymbol{\eta}_b) \mathbf{u} \tag{11}$$

where

$$\mathbf{D}(\boldsymbol{\xi}) \in \mathbb{R}^{6\times 6} \triangleq \begin{bmatrix} m\mathbf{I}_{3\times 3} & \mathbf{0}_{3\times 3} \\ \mathbf{0}_{3\times 3} & \mathbf{M}(\boldsymbol{\eta}_b) \end{bmatrix}$$

is the inertial forces matrix with m representing the scalar total mass of the UAV, $\mathbf{I}_{n\times n}$ denotes the $n \times n$ identity, $\mathbf{0}_n$ is the n-dimensional zero vector or matrix,

$$\mathbf{M}(\boldsymbol{\eta}_b) \in \mathbb{R}^{3\times 3} \triangleq \begin{bmatrix} 1 & 0 & -s_\theta \\ 0 & c_\phi & c_\theta s_\phi \\ 0 & -s_\phi & c_\theta c_\phi \end{bmatrix}^T \underbrace{\operatorname{diag}(J_{xx}, J_{yy}, J_{zz})}_{\mathbf{J}_b} \underbrace{\begin{bmatrix} 1 & 0 & -s_\theta \\ 0 & c_\phi & c_\theta s_\phi \\ 0 & -s_\phi & c_\theta c_\phi \end{bmatrix}}_{\mathbf{Q}(\boldsymbol{\eta}_b)},$$

$\mathbf{J}_b$ is the inertia tensor of the airframe with $J_{xx}, J_{yy}, J_{zz} > 0$, $c_{(\cdot)}$ and $s_{(\cdot)}$ denote the cosine and sine functions, respectively; furthermore,

$$\mathbf{C}(\boldsymbol{\xi}, \dot{\boldsymbol{\xi}}) \in \mathbb{R}^{6\times 6} \triangleq \begin{bmatrix} \mathbf{0}_{3\times 3} & \mathbf{0}_{3\times 3} \\ \mathbf{0}_{3\times 3} & \mathbf{Q}(\boldsymbol{\eta}_b)^T \mathbf{S}_\times(\mathbf{Q}(\boldsymbol{\eta}_b)\dot{\boldsymbol{\eta}}_b)\mathbf{J}_b\mathbf{Q}(\boldsymbol{\eta}_b) + \mathbf{Q}(\boldsymbol{\eta}_b)^T\mathbf{J}_b\dot{\mathbf{Q}}(\boldsymbol{\eta}_b) \end{bmatrix}$$

is the centrifugal and Coriolis forces matrix with $\mathbf{S}_\times$ denoting the skew symmetric operator, $\mathbf{g} \in \mathbb{R}^6 \triangleq \begin{bmatrix} \mathbf{0}_2^T & -mg & \mathbf{0}_3^T \end{bmatrix}^T$ is the gravity forces vector, $\boldsymbol{\Gamma}(\boldsymbol{\eta}_b) \in \mathbb{R}^{6\times 6} \triangleq$ blockdiag$\left(\mathbf{R}_b(\boldsymbol{\eta}_b), \mathbf{Q}(\boldsymbol{\eta}_b)^T\right)$, with

$$\mathbf{R}_b(\boldsymbol{\eta}_b) \in \mathcal{SO}(3) \triangleq \begin{bmatrix} c_\theta c_\psi & s_\phi\, s_\theta c_\psi - c_\phi s_\psi & c_\phi\, s_\theta c_\psi + s_\phi s_\psi \\ c_\theta s_\psi & s_\phi\, s_\theta s_\psi + c_\phi c_\psi & c_\phi\, s_\theta s_\psi - s_\phi c_\psi \\ -s_\theta & s_\phi c_\theta & c_\phi c_\theta \end{bmatrix},$$

$\mathbf{u} \in \mathbb{R}^6$ is the control wrench and $\mathbf{w}_e(\cdot) \in \mathbb{R}^6$ is the external wrench that might depend or not on time or other factors, and for such a reason its explicit dependency is dropped hereafter, namely $\mathbf{w}_e(\cdot) = \mathbf{w}_e$. The full derivation of Euqation (11) is available in [17]. Next, some useful properties of the UAV dynamics are presented.

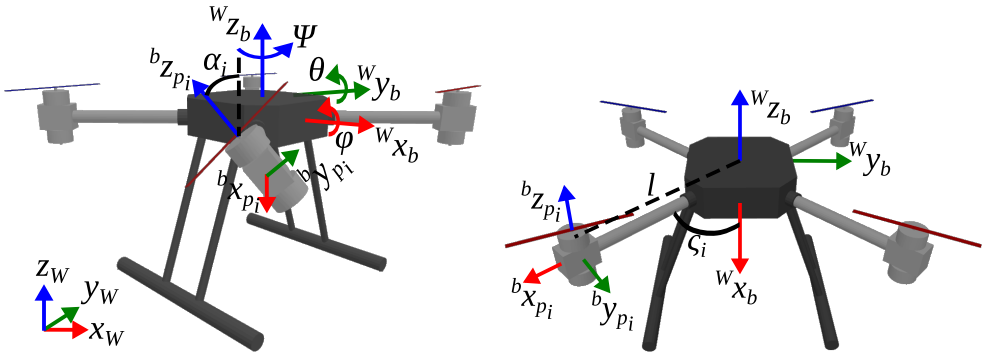

Figure 1. Actively tilting quadrotor. Left: projected view. Right: front and top view.

Properties and Assumptions of the Actively Tilting Quadrotor Dynamics

Property 1. *Property 1. The matrix* $\mathbf{D}(\boldsymbol{\xi})$ *is symmetric, positive definite and invertible within the range* $-\pi/2 < \theta < \pi/2$ *[17].*

Property 2. *There exist scalar positive constants* $\gamma_{\mathbf{D}(\xi)}$, $\gamma_{\mathbf{C}(\xi,\dot{\xi})}$, $\gamma_{\mathbf{g}}$ *and* $\mathbf{w}_e$ *such that*

$$\|\mathbf{D}(\boldsymbol{\xi})\| \leq \gamma_{\mathbf{D}(\xi)}, \tag{12}$$

$$\mathbf{C}(\boldsymbol{\xi}, \dot{\boldsymbol{\xi}})\dot{\boldsymbol{\xi}} \leq \|\mathbf{C}(\boldsymbol{\xi}, \dot{\boldsymbol{\xi}})\|\|\dot{\boldsymbol{\xi}}\| \leq \gamma_{\mathbf{C}(\xi,\dot{\xi})}\|\dot{\boldsymbol{\xi}}\|, \tag{13}$$

$$\|\mathbf{g}\| \leq \gamma_{\mathbf{g}}, \tag{14}$$

$$\|\mathbf{w}_e\| \leq \gamma_{\mathbf{w}_e}. \tag{15}$$

Property 3. *Using the appropriate representations, the* $\mathbf{D}(\boldsymbol{\xi})$ *and* $\mathbf{C}(\boldsymbol{\xi}, \dot{\boldsymbol{\xi}})$ *matrices satisfy [17]*

$$\mathbf{x}^T\left(\frac{1}{2}\dot{\mathbf{D}}(\boldsymbol{\xi}) - \mathbf{C}(\boldsymbol{\xi}, \dot{\boldsymbol{\xi}})\right)\mathbf{x} = 0, \ \forall\, \mathbf{x} \in \mathbb{R}^6, \tag{16}$$

which is known as the skew symmetric property; moreover

$$\dot{\mathbf{D}}(\boldsymbol{\xi}) = \mathbf{C}(\boldsymbol{\xi}, \dot{\boldsymbol{\xi}})^T + \mathbf{C}(\boldsymbol{\xi}, \dot{\boldsymbol{\xi}}). \tag{17}$$

Assumption 1. *The accurate measurement of the full pose* $\boldsymbol{\xi}$ *is available.*

Assumption 2. *As a consequence of the "X" configuration of the actively tilting quadrotor, its allowable configuration space is restricted to $-\pi/2 < \theta < \pi/2$; therefore, it will not be employed either for acrobatic manoeuvres nor for other tasks demanding the UAV to abandon its allowable configuration space [17]; in fact, it is desired that the actively tilting quadrotor always work with zero orientation by exploiting its tilting propellers property to perform translational motions.*

4. Hyperbolic Control for Robust Flight

The main objective of a globally attractive control system is to lead the solutions of the differential equations representing a closed-loop system towards a determined existing or virtual equilibrium point, notwithstanding how far from the origin the initial conditions of the system would be. In the worst case, the solutions must converge to a close vicinity (or ball) about the equilibrium and never leave it. In this context, considering the dynamics of the actively tiling quadrotor Equation (11), a control problem is to achieve a constant set point or a trajectory and remain closely about it, despite possible disturbances and no matter how far it is. Mathematically, in terms of the pose error $\tilde{\boldsymbol{\xi}} \in \mathbb{R}^6 \triangleq \boldsymbol{\xi}^d - \boldsymbol{\xi}$, the control objective can be expressed as

$$\left\| \tilde{\boldsymbol{\xi}}, \dot{\tilde{\boldsymbol{\xi}}} \right\| \leq r \simeq 0 \; \forall \; t > t_c > 0, \tag{18}$$

where r is a scalar representing the radius of an origin-centred ball $\mathbf{B}r$, and t_c denotes a convergence time. Therefore, to overcome this challenge, the proposed controller is

$$\mathbf{u} = \boldsymbol{\Gamma}(\boldsymbol{\eta}_b)^{-1}\left[\mathbf{K}_p \mathbf{tanh}\left(\tilde{\boldsymbol{\xi}}\right) + \mathbf{K}_i \mathbf{tanh}(\boldsymbol{\varrho}) + \mathbf{K}_v \dot{\tilde{\boldsymbol{\xi}}} + \dot{\boldsymbol{\xi}}^d + \ddot{\boldsymbol{\xi}}^d\right] \tag{19}$$

where $\boldsymbol{\varrho} = \int_0^t \tilde{\boldsymbol{\xi}}(\vartheta)\, d\vartheta$ with ϑ denotes a time interval, $\mathbf{tanh}\left(\tilde{\boldsymbol{\xi}}\right)$ is a six-dimensional vector function as in Euqation (2), and $\mathbf{K}_p,\ \mathbf{K}_i,\ \mathbf{K}_v \in \mathbb{R}^{6\times 6}$ are diagonal with positive entries that must be chosen to satisfy

$$\lambda_{\min}\left\{\mathbf{K}_p\right\} \geq \lambda_{\min}\{\mathbf{K}_v\} > \gamma_{\mathbf{C}(\boldsymbol{\xi},\dot{\boldsymbol{\xi}})}, \tag{20}$$

$$\sqrt{6}\lambda_{\min}\{\mathbf{K}_i\} > \gamma_{\mathbf{g}} + \gamma_{\mathbf{w}_e}. \tag{21}$$

$\lambda_{\min}\{\cdot\}$ denotes the minimum or smallest eigenvalue. Thus, the error dynamics or closed-loop system representation is

$$\begin{bmatrix} \dot{\tilde{\boldsymbol{\xi}}} \\ \ddot{\tilde{\boldsymbol{\xi}}} \end{bmatrix} = \begin{bmatrix} \dot{\boldsymbol{\xi}}^d - \dot{\boldsymbol{\xi}} \\ \ddot{\boldsymbol{\xi}}^d \mathbf{D}(\boldsymbol{\xi})^{-1}\Big[\boldsymbol{\Gamma}(\boldsymbol{\eta}_b)^{-1}\Big(\mathbf{K}_p \mathbf{tanh}\left(\tilde{\boldsymbol{\xi}}\right) + \mathbf{K}_i \mathbf{tanh}(\boldsymbol{\varrho}) + \mathbf{K}_v \dot{\tilde{\boldsymbol{\xi}}} + \dot{\boldsymbol{\xi}}^d + \ddot{\boldsymbol{\xi}}^d\Big) \\ -\mathbf{C}(\boldsymbol{\xi}, \dot{\boldsymbol{\xi}})\dot{\boldsymbol{\xi}} - \mathbf{g} - \mathbf{w}_e\Big] \end{bmatrix} \tag{22}$$

Further down, given the properties and assumptions of the actively tilting quadrotor dynamics, it is demonstrated that a close vicinity about the origin of the solutions of the closed-loop differential equations is globally attractive.

4.1. Globally Attractive Ultimate Boundedness

Theorem 1. *Under Assumptions 1 and 2, the solutions of Equation (22) are globally attracted to a vicinity of the origin and remain there after reaching it.*

Proof. Consider the following candidate Lyapunov function

$$V\left(\tilde{\boldsymbol{\xi}}, \dot{\tilde{\boldsymbol{\xi}}}\right) = \frac{1}{2}\dot{\tilde{\boldsymbol{\xi}}}^T \mathbf{D}(\boldsymbol{\xi})\dot{\tilde{\boldsymbol{\xi}}} + \boldsymbol{\varsigma}\left(\tilde{\boldsymbol{\xi}}\right)^T \mathbf{K}_p \boldsymbol{\varsigma}\left(\tilde{\boldsymbol{\xi}}\right) + \frac{\epsilon_0}{1 + \|\tilde{\boldsymbol{\xi}}\|}\tilde{\boldsymbol{\xi}}^T \mathbf{D}(\boldsymbol{\xi})\dot{\tilde{\boldsymbol{\xi}}}, \tag{23}$$

where ϵ_0 is a positive scalar and $\varsigma(\tilde{\xi}) : \mathbb{R}^6 \to \mathbb{R}^6$ is a vector function such as Equation (6). Notice that $V\left(\tilde{\xi}, \dot{\tilde{\xi}}\right)$ is positive definite and radially unbounded [18]. The time derivative of $V\left(\tilde{\xi}, \dot{\tilde{\xi}}\right)$ is

$$\begin{aligned}\dot{V}\left(\tilde{\xi}, \dot{\tilde{\xi}}\right) = \; & \dot{\tilde{\xi}}^T \mathbf{D}(\xi)\ddot{\tilde{\xi}} + \frac{1}{2}\dot{\tilde{\xi}}^T \dot{\mathbf{D}}(\xi)\dot{\tilde{\xi}} + 2\varsigma(\tilde{\xi})^T \mathbf{K}_p \dot{\varsigma}(\tilde{\xi}) - \frac{\epsilon_0}{\|\tilde{\xi}\|\left[1+\|\tilde{\xi}\|\right]^2}\tilde{\xi}^T \dot{\tilde{\xi}}\tilde{\xi}^T \mathbf{D}(\xi)\dot{\tilde{\xi}} \\ & + \frac{\epsilon_0}{1+\|\tilde{\xi}\|}\dot{\tilde{\xi}}^T \mathbf{D}(\xi)\dot{\tilde{\xi}} + \frac{\epsilon_0}{1+\|\tilde{\xi}\|}\tilde{\xi}^T \dot{\mathbf{D}}(\xi)\dot{\tilde{\xi}} + \frac{\epsilon_0}{1+\|\tilde{\xi}\|}\tilde{\xi}^T \mathbf{D}(\xi)\ddot{\tilde{\xi}}.\end{aligned} \tag{24}$$

Substituting the UAV dynamics Equation (11) in $\dot{V}\left(\tilde{\xi}, \dot{\tilde{\xi}}\right)$ yields

$$\begin{aligned}\dot{V}\left(\tilde{\xi}, \dot{\tilde{\xi}}\right) = \; & \dot{\tilde{\xi}}^T \mathbf{D}(\xi)\ddot{\xi}^d - \dot{\tilde{\xi}}^T\left[\mathbf{\Gamma}(\eta_b)\mathbf{u} - \mathbf{C}(\xi,\dot{\xi})\dot{\xi} - \mathbf{g} - \mathbf{w}_e\right] + \frac{1}{2}\dot{\tilde{\xi}}^T \dot{\mathbf{D}}(\xi)\dot{\tilde{\xi}} + \\ & 2\varsigma(\tilde{\xi})^T \mathbf{K}_p \dot{\varsigma}(\tilde{\xi}) - \frac{\epsilon_0}{\|\tilde{\xi}\|\left[1+\|\tilde{\xi}\|\right]^2}\tilde{\xi}^T \dot{\tilde{\xi}}\tilde{\xi}^T \mathbf{D}(\xi)\dot{\tilde{\xi}} + \\ & \frac{\epsilon_0}{1+\|\tilde{\xi}\|}\dot{\tilde{\xi}}^T \mathbf{D}(\xi)\dot{\tilde{\xi}} + \frac{\epsilon_0}{1+\|\tilde{\xi}\|}\tilde{\xi}^T \dot{\mathbf{D}}(\xi)\dot{\tilde{\xi}} + \frac{\epsilon_0}{1+\|\tilde{\xi}\|}\tilde{\xi}^T \mathbf{D}(\xi)\ddot{\xi}^d - \\ & \frac{\epsilon_0}{1+\|\tilde{\xi}\|}\tilde{\xi}^T\left[\mathbf{\Gamma}(\eta_b)\mathbf{u} - \mathbf{C}(\xi,\dot{\xi})\dot{\xi} - \mathbf{g} - \mathbf{w}_e\right].\end{aligned} \tag{25}$$

Provided that $\dot{\tilde{\xi}} = \dot{\xi}^d - \dot{\tilde{\xi}}$, $\dot{V}\left(\tilde{\xi}, \dot{\tilde{\xi}}\right)$ can be rewritten as

$$\begin{aligned}\dot{V}\left(\tilde{\xi}, \dot{\tilde{\xi}}\right) = \; & \dot{\tilde{\xi}}^T \mathbf{D}(\xi)\ddot{\xi}^d - \dot{\tilde{\xi}}^T\left[\mathbf{\Gamma}(\eta_b)\mathbf{u} - \mathbf{C}(\xi,\dot{\xi})\dot{\xi}^d - \mathbf{g} - \mathbf{w}_e\right] + \\ & \dot{\tilde{\xi}}^T\left(\frac{1}{2}\dot{\mathbf{D}}(\xi)\dot{\tilde{\xi}} - \mathbf{C}(\xi,\dot{\xi})\right)\dot{\tilde{\xi}} + 2\varsigma(\tilde{\xi})^T \mathbf{K}_p \dot{\varsigma}(\tilde{\xi}) - \\ & \frac{\epsilon_0}{\|\tilde{\xi}\|\left[1+\|\tilde{\xi}\|\right]^2}\tilde{\xi}^T \dot{\tilde{\xi}}\tilde{\xi}^T \mathbf{D}(\xi)\dot{\tilde{\xi}} + \frac{\epsilon_0}{1+\|\tilde{\xi}\|}\dot{\tilde{\xi}}^T \mathbf{D}(\xi)\dot{\tilde{\xi}} + \\ & \frac{\epsilon_0}{1+\|\tilde{\xi}\|}\tilde{\xi}^T \dot{\mathbf{D}}(\xi)\dot{\tilde{\xi}} + \frac{\epsilon_0}{1+\|\tilde{\xi}\|}\tilde{\xi}^T \mathbf{D}(\xi)\ddot{\xi}^d - \\ & \frac{\epsilon_0}{1+\|\tilde{\xi}\|}\tilde{\xi}^T\left[\mathbf{\Gamma}(\eta_b)\mathbf{u} - \mathbf{C}(\xi,\dot{\xi})\dot{\xi}^d - \mathbf{g} - \mathbf{w}_e\right] - \\ & \frac{\epsilon_0}{1+\|\tilde{\xi}\|}\tilde{\xi}^T \mathbf{C}(\xi,\dot{\xi})\dot{\tilde{\xi}}.\end{aligned} \tag{26}$$

Then, taking into account Equations (7), (16) and (17), after some algebra it follows that

$$\begin{aligned}\dot{V}\left(\tilde{\xi}, \dot{\tilde{\xi}}\right) = \; & \dot{\tilde{\xi}}^T \mathbf{D}(\xi)\ddot{\xi}^d - \dot{\tilde{\xi}}^T\left[\mathbf{\Gamma}(\eta_b)\mathbf{u} - \mathbf{C}(\xi,\dot{\xi})\dot{\xi}^d - \mathbf{g} - \mathbf{w}_e\right] + \dot{\tilde{\xi}}^T \mathbf{K}_p \mathbf{tanh}(\tilde{\xi}) - \\ & \frac{\epsilon_0}{\|\tilde{\xi}\|\left[1+\|\tilde{\xi}\|\right]^2}\tilde{\xi}^T \dot{\tilde{\xi}}\tilde{\xi}^T \mathbf{D}(\xi)\dot{\tilde{\xi}} + \frac{\epsilon_0}{1+\|\tilde{\xi}\|}\dot{\tilde{\xi}}^T \mathbf{D}(\xi)\dot{\tilde{\xi}} + \\ & \frac{\epsilon_0}{1+\|\tilde{\xi}\|}\tilde{\xi}^T \mathbf{C}(\xi,\dot{\xi})^T\dot{\tilde{\xi}} + \frac{\epsilon_0}{1+\|\tilde{\xi}\|}\tilde{\xi}^T \mathbf{D}(\xi)\ddot{\xi}^d - \\ & \frac{\epsilon_0}{1+\|\tilde{\xi}\|}\tilde{\xi}^T\left[\mathbf{\Gamma}(\eta_b)\mathbf{u} - \mathbf{C}(\xi,\dot{\xi})\dot{\xi}^d - \mathbf{g} - \mathbf{w}_e\right].\end{aligned} \tag{27}$$

Folding Equation (19) into $\dot{V}\left(\tilde{\xi},\dot{\tilde{\xi}}\right)$ yields

$$\begin{aligned}\dot{V}\left(\tilde{\xi},\dot{\tilde{\xi}}\right) = \;& \dot{\tilde{\xi}}^T\mathbf{D}(\xi)\ddot{\xi}^d - \dot{\tilde{\xi}}^T\Big[\mathbf{K}_p\mathbf{tanh}\left(\tilde{\xi}\right) + \mathbf{K}_i\mathbf{tanh}(\varrho) + \mathbf{K}_v\dot{\tilde{\xi}} + \ddot{\xi}^d + \\ & \dot{\xi}^d - \mathbf{C}(\xi,\dot{\xi})\dot{\xi}^d - \mathbf{g} - \mathbf{w}_e\Big] + \dot{\tilde{\xi}}^T\mathbf{K}_p\mathbf{tanh}\left(\tilde{\xi}\right) - \\ & \frac{\epsilon_0}{\|\tilde{\xi}\|\left[1+\|\tilde{\xi}\|\right]^2}\tilde{\xi}^T\dot{\tilde{\xi}}\tilde{\xi}^T\mathbf{D}(\xi)\dot{\tilde{\xi}} + \frac{\epsilon_0}{1+\|\tilde{\xi}\|}\dot{\tilde{\xi}}^T\mathbf{D}(\xi)\dot{\tilde{\xi}} + \\ & \frac{\epsilon_0}{1+\|\tilde{\xi}\|}\tilde{\xi}^T\mathbf{C}(\xi,\dot{\xi})^T\dot{\tilde{\xi}} + \frac{\epsilon_0}{1+\|\tilde{\xi}\|}\tilde{\xi}^T\mathbf{D}(\xi)\ddot{\xi}^d - \\ & \frac{\epsilon_0}{1+\|\tilde{\xi}\|}\tilde{\xi}^T\Big[\mathbf{K}_p\mathbf{tanh}\left(\tilde{\xi}\right) + \mathbf{K}_i\mathbf{tanh}(\varrho) + \mathbf{K}_v\dot{\tilde{\xi}} + \ddot{\xi}^d + \\ & \dot{\xi}^d - \mathbf{C}(\xi,\dot{\xi})\dot{\xi}^d - \mathbf{g} - \mathbf{w}_e\Big],\end{aligned} \tag{28}$$

and then rearranging some terms

$$\begin{aligned}\dot{V}\left(\tilde{\xi},\dot{\tilde{\xi}}\right) = \;& \dot{\tilde{\xi}}^T\left[\frac{\epsilon_0}{1+\|\tilde{\xi}\|}\mathbf{D}(\xi) - \mathbf{K}_v\right]\dot{\tilde{\xi}} - \dot{\tilde{\xi}}^T[\mathbf{K}_i\mathbf{tanh}(\varrho) - \mathbf{g} - \mathbf{w}_e] + \\ & \dot{\tilde{\xi}}^T[\mathbf{D}(\xi) - \mathbf{I}_{6\times6}]\ddot{\xi}^d + \dot{\tilde{\xi}}^T\left[\mathbf{C}(\xi,\dot{\xi}) - \mathbf{I}_{6\times6}\right]\dot{\xi}^d - \\ & \frac{\epsilon_0}{\|\tilde{\xi}\|\left[1+\|\tilde{\xi}\|\right]^2}\tilde{\xi}^T\dot{\tilde{\xi}}\tilde{\xi}^T\mathbf{D}(\xi)\dot{\tilde{\xi}} + \frac{\epsilon_0}{1+\|\tilde{\xi}\|}\tilde{\xi}^T\mathbf{C}(\xi,\dot{\xi})^T\dot{\tilde{\xi}} + \\ & \frac{\epsilon_0}{1+\|\tilde{\xi}\|}\tilde{\xi}^T[\mathbf{D}(\xi) - \mathbf{I}_{6\times6}]\ddot{\xi}^d + \frac{\epsilon_0}{1+\|\tilde{\xi}\|}\tilde{\xi}^T\left[\mathbf{C}(\xi,\dot{\xi}) - \mathbf{I}_{6\times6}\right]\dot{\xi}^d \\ & - \frac{\epsilon_0}{1+\|\tilde{\xi}\|}\tilde{\xi}^T\Big[\mathbf{K}_p\mathbf{tanh}\left(\tilde{\xi}\right) + \mathbf{K}_i\mathbf{tanh}(\varrho) + \mathbf{K}_v\dot{\tilde{\xi}} - \mathbf{g} - \mathbf{w}_e\Big].\end{aligned} \tag{29}$$

Now, Equations (3)–(5) bring about the following inequalities

$$\begin{aligned}\dot{\tilde{\xi}}^T\left[\frac{\epsilon_0}{1+\|\tilde{\xi}\|}\mathbf{D}(\xi) - \mathbf{K}_v\right]\dot{\tilde{\xi}} &\leq [\epsilon_0\|\mathbf{D}(\xi)\| - \|\mathbf{K}_v\|]\left\|\dot{\tilde{\xi}}\right\|^2, \\ -\dot{\tilde{\xi}}^T[\mathbf{K}_i\mathbf{tanh}(\varrho) - \mathbf{g} - \mathbf{w}_e] &\leq -\left[\sqrt{6}\|\mathbf{K}_i\| - \|\mathbf{g}\| - \|\mathbf{w}_e\|\right]\left\|\dot{\tilde{\xi}}\right\|, \\ \dot{\tilde{\xi}}^T[\mathbf{D}(\xi) - \mathbf{I}_{6\times6}]\ddot{\xi}^d &\leq [\|\mathbf{D}(\xi)\| - 1]\left\|\ddot{\xi}^d\right\|\left\|\dot{\tilde{\xi}}\right\|, \\ \dot{\tilde{\xi}}^T\left[\mathbf{C}(\xi,\dot{\xi}) - \mathbf{I}_{6\times6}\right]\dot{\xi}^d &\leq [\|\mathbf{C}(\xi,\dot{\xi})\| - 1]\left\|\dot{\xi}^d\right\|\left\|\dot{\tilde{\xi}}\right\|,\end{aligned}$$

$$-\frac{\epsilon_0\tilde{\xi}^T\dot{\tilde{\xi}}\tilde{\xi}^T\mathbf{D}(\xi)\dot{\tilde{\xi}}}{\|\tilde{\xi}\|\left[1+\|\tilde{\xi}\|\right]^2} \leq -\frac{\epsilon_0\|\mathbf{D}(\xi)\|\|\tilde{\xi}\|^2\left\|\dot{\tilde{\xi}}\right\|^2}{\|\tilde{\xi}\|\left[1+\|\tilde{\xi}\|\right]^2} \leq -\epsilon_0\|\mathbf{D}(\xi)\|\left\|\dot{\tilde{\xi}}\right\|^2,$$

$$\begin{aligned}\frac{\epsilon_0}{1+\|\tilde{\xi}\|}\tilde{\xi}^T\mathbf{C}(\xi,\dot{\xi})^T\dot{\tilde{\xi}} &\leq \epsilon_0\|\mathbf{C}(\xi,\dot{\xi})\|\|\tilde{\xi}\|\left\|\dot{\tilde{\xi}}\right\|, \\ \frac{\epsilon_0}{1+\|\tilde{\xi}\|}\tilde{\xi}^T[\mathbf{D}(\xi) - \mathbf{I}_{6\times6}]\ddot{\xi}^d &\leq \epsilon_0[\|\mathbf{D}(\xi)\| - 1]\left\|\ddot{\xi}^d\right\|\|\tilde{\xi}\|, \\ \frac{\epsilon_0}{1+\|\tilde{\xi}\|}\tilde{\xi}^T\left[\mathbf{C}(\xi,\dot{\xi}) - \mathbf{I}_{6\times6}\right]\dot{\xi}^d &\leq \epsilon_0\left[\|\mathbf{C}(\xi,\dot{\xi})\| - 1\right]\left\|\dot{\xi}^d\right\|\|\tilde{\xi}\|, \\ -\frac{\epsilon_0}{1+\|\tilde{\xi}\|}\tilde{\xi}^T\mathbf{K}_v\dot{\tilde{\xi}} &\leq -\epsilon_0\|\mathbf{K}_v\|\|\tilde{\xi}\|\left\|\dot{\tilde{\xi}}\right\|, \\ -\frac{\epsilon_0}{1+\|\tilde{\xi}\|}\tilde{\xi}^T[\mathbf{K}_i\mathbf{tanh}(\varrho) - \mathbf{g} - \mathbf{w}_e] &\leq -\epsilon_0\left[\sqrt{6}\|\mathbf{K}_i\| - \|\mathbf{g}\| - \|\mathbf{w}_e\|\right]\|\tilde{\xi}\|, \\ -\frac{\epsilon_0}{1+\|\tilde{\xi}\|}\tilde{\xi}^T\mathbf{K}_p\mathbf{tanh}\left(\tilde{\xi}\right) &\leq -\epsilon_0\|\mathbf{K}_p\|\|\tilde{\xi}\|^2.\end{aligned}$$

Considering the aforesaid inequalities as well as the bounds Equations (12)–(15), then $\dot{V}\left(\tilde{\xi},\dot{\tilde{\xi}}\right)$ becomes

$$\dot{V}\left(\tilde{\xi},\dot{\tilde{\xi}}\right) \leq -\epsilon_0 \begin{bmatrix} \|\tilde{\xi}\| \\ \|\dot{\tilde{\xi}}\| \end{bmatrix}^T \underbrace{\begin{bmatrix} \|\mathbf{K}_p\| & -\frac{\left[\gamma_{\mathbf{C}(\xi,\dot{\xi})} - \|\mathbf{K}_v\|\right]}{2} \\ -\frac{\left[\gamma_{\mathbf{C}(\xi,\dot{\xi})} - \|\mathbf{K}_v\|\right]}{2} & \frac{\|\mathbf{K}_v\|}{\epsilon_0} \end{bmatrix}}_{\mathbf{A}} \begin{bmatrix} \|\tilde{\xi}\| \\ \|\dot{\tilde{\xi}}\| \end{bmatrix} + \underbrace{\begin{bmatrix} \epsilon_0\left(-\sqrt{6}\|\mathbf{K}_i\| + \gamma_{\mathbf{g}} + \gamma_{\mathbf{w}_e} + \left[\gamma_{\mathbf{D}(\xi)} - 1\right]\left\|\ddot{\xi}^d\right\| + \left[\gamma_{\mathbf{C}(\xi,\dot{\xi})} - 1\right]\left\|\dot{\xi}^d\right\|\right) \\ -\sqrt{6}\|\mathbf{K}_i\| + \gamma_{\mathbf{g}} + \gamma_{\mathbf{w}_e} + \left[\gamma_{\mathbf{D}(\xi)} - 1\right]\left\|\ddot{\xi}^d\right\| + \left[\gamma_{\mathbf{C}(\xi,\dot{\xi})} - 1\right]\left\|\dot{\xi}^d\right\| \end{bmatrix}}_{\mathbf{b}}^T \begin{bmatrix} \|\tilde{\xi}\| \\ \|\dot{\tilde{\xi}}\| \end{bmatrix}. \tag{30}$$

Therefore, the solutions are globally attracted to the bounded ball $\mathbf{B}_r = \left\{ \left[\tilde{\xi}\ \dot{\tilde{\xi}}\right]^T \in \mathbb{R}^{12} : \left\| \left[\tilde{\xi}\ \dot{\tilde{\xi}}\right]^T \right\| \leq \|\mathbf{b}\| \right\}$ because $\mathbf{A}$ is positive definite due to Equation (20) and therefore $\dot{V}\left(\tilde{\xi},\dot{\tilde{\xi}}\right)$ is negative definite as a consequence of Equation (21). Moreover, notice that $\|\mathbf{b}\|$ can be considerably reduced by properly tuning $\mathbf{K}_i$ and selecting a suitable desired trajectory. □

4.2. Control Allocation

Consider Figure 1. The position and orientation of the coordinate frame of each rotor with respect to the airframe are

$$\mathbf{p}_{p_i} \in \mathbb{R}^3 \triangleq \begin{bmatrix} {}^W x_{p_i} & {}^W y_{p_i} & {}^W z_{p_i} \end{bmatrix}^T = l\mathbf{R}_z(\varsigma_i)\mathbf{e}_1 \tag{31}$$

$$\mathbf{R}_{p_i}(\alpha_i(t)) \in \mathcal{SO}3 = \mathbf{R}_z(\varsigma_i)\mathbf{R}_x(\alpha_i(t)), \tag{32}$$

with $i = 1,2,3,4$; $\mathbf{R}_{(\cdot)} \in \mathcal{SO}3$ are rotation matrices, ς_i is a scalar constant angle and $(-1)^{i-1}\alpha_i(t)$ is scalar and variable; l is the constant scalar length of each boom of the UAV and $\mathbf{e}_1 = [1\ 0\ 0]^T$. Provided that the actively tilting quadrotor is in the "X" configuration, then $\varsigma_{1,2,3,4} = \{\pi/4,\ 3\pi/4, -3\pi/4, -\pi/4\}$. The forces and torques exerted by each propeller are therefore given by [19]

$$\mathbf{f}_{p_i} \in \mathbb{R}^3 = T_i\mathbf{R}_{p_i}(\alpha_i(t))\mathbf{e}_3 \tag{33}$$

$$\boldsymbol{\tau}_{p_i} \in \mathbb{R}^3 = \left[\mathbf{p}_{p_i} \times T_i\mathbf{R}_{p_i}(\alpha_i(t))\right] + \left[(-1)^{i-1}T_i\mathbf{R}_{p_i}(\alpha_i(t))\mathbf{e}_3\right], \tag{34}$$

where $i = 1,2,3,4$; $T_i \in \mathbb{R} = k_f\omega_i^2$ is the thrust exerted by the ith propeller due to its scalar angular speed ω_i; k_f, k_τ and $\sigma = k_\tau/k_f$ are positive scalar constant coefficients related to the geometry of the propellers and $\mathbf{e}_3 = [0\ 0\ 1]^T$. Hence, the control wrench of the UAV retrieved from the total forces Equation (33) and torques Equation (34) exerted by the rotors is

$$\mathbf{u} = \begin{bmatrix} \sum_{i=1}^{4} \mathbf{f}_{R_i}^T & \sum_{i=1}^{4} \boldsymbol{\tau}_{R_i}^T \end{bmatrix}^T. \tag{35}$$

However, the angle $\alpha_i(t)$ vectorizes the thrust T_i yielding its decomposition as $T_i = T_{i_z}\cos(\alpha_i(t)) + T_{i_{xy}}\sin(\alpha_i(t))$. Then, from Equations (31) and (32), the following relation can be obtained

$$\mathbf{u} = k_f \underbrace{\begin{bmatrix} 0 & 0 & 0 & 0 & \frac{1}{\sqrt{2}} & \frac{1}{\sqrt{2}} & -\frac{1}{\sqrt{2}} & -\frac{1}{\sqrt{2}} \\ 0 & 0 & 0 & 0 & -\frac{1}{\sqrt{2}} & \frac{1}{\sqrt{2}} & \frac{1}{\sqrt{2}} & -\frac{1}{\sqrt{2}} \\ 1 & 1 & 1 & 1 & 0 & 0 & 0 & 0 \\ \frac{l}{\sqrt{2}} & \frac{l}{\sqrt{2}} & -\frac{l}{\sqrt{2}} & -\frac{l}{\sqrt{2}} & \frac{\sigma}{\sqrt{2}} & -\frac{\sigma}{\sqrt{2}} & -\frac{\sigma}{\sqrt{2}} & \frac{\sigma}{\sqrt{2}} \\ -\frac{l}{\sqrt{2}} & \frac{l}{\sqrt{2}} & \frac{l}{\sqrt{2}} & -\frac{l}{\sqrt{2}} & -\frac{\sigma}{\sqrt{2}} & -\frac{\sigma}{\sqrt{2}} & \frac{\sigma}{\sqrt{2}} & \frac{\sigma}{\sqrt{2}} \\ \sigma & -\sigma & \sigma & -\sigma & -l & -l & -l & -l \end{bmatrix}}_{\mathbf{\Lambda}} \begin{bmatrix} T_{1_z} \\ T_{2_z} \\ T_{3_z} \\ T_{4_z} \\ T_{1_{xy}} \\ T_{2_{xy}} \\ T_{3_{xy}} \\ T_{4_{xy}} \end{bmatrix}. \tag{36}$$

Notice that whenever $\alpha_i(t)$ is zero, the xy component of the thrust is also zero. Furthermore, the angular speed and the tilting angle of each propeller that compose the controller $\mathbf{u}$ can be retrieved through the equations below

$$\begin{bmatrix} T_{1_z} & T_{2_z} & T_{3_z} & T_{4_z} & T_{1_{xy}} & T_{2_{xy}} & T_{3_{xy}} & T_{4_{xy}} \end{bmatrix}^T = \mathbf{\Lambda}^+ \mathbf{u} \tag{37}$$

$$T_i = \sqrt{T_{i_z}^2 + T_{i_{xy}}^2} \tag{38}$$

$$\omega_i = \sqrt{\frac{T_i}{k_f}} \tag{39}$$

$$\alpha_i(t) = \tan^{-1}\left(\frac{T_{i_z}}{T_{i_{xy}}}\right) \tag{40}$$

5. Physics-Engine-Based Simulation Results

This section describes the experiments carried out to evaluate the performance and effectiveness of the proposed control system. In the first place, the physics-engine-based simulation setup is described and afterwards, the tracking and regulation experiments upon adverse conditions are detailed as well as the comparison against a state-of-the-art controller. A video containing all the aforementioned experiments is available at https://youtu.be/IypBZoISHvM (Accessed on 2 November 2022).

5.1. Implementation of the Controller

Different from the results presented in the literature, the proposed control system was implemented in a virtual model of an actively tilting quadrotor that is simulated within the physics-engine-based simulator *Gazebo*. This type of simulation provides more realistic results than traditional numerical methods in view of the fact that several physical phenomena are included by default, such as the gravity or contacts for instance; in contrast, each phenomenon should be included in a numerical simulation algorithm in order to observe their effects on the system studied. In the case of this work, the aerodynamics of the propellers and the actuator dynamics were present in the simulation scheme through the use of the library *RotorS* (https://github.com/ethz-asl/rotors_simulator/wiki (Accessed on 2 November 2022)). As a consequence, our simulation system provided a behaviour that was almost identical to a real UAV, which also represented a better test bench for the proposed controller.

The actively tilting quadrotor model was developed using the *Unified Robot Description Format* (URDF), and it was put into effect within the *Gazebo* simulator by means of the *Robotics Operating System* (ROS). This scheme works as follows: the virtual model of the UAV is equipped with sensors and actuators whose input and output signals are accessed through the ROS messaging system, which is helpful to compute several algorithms in

parallel. In this regard, the feedback from the UAV, namely the full pose $\boldsymbol{\xi}$, is available; in addition, the actuators of the UAV consist of the rotors actuating the propellers and position-controlled servomotors that are useful to tilt them. Hence, the propellers require the command of the angular speed ω_i and the servomotors receive the desired angular position α_i.

Now, since the feedback and actuation systems were accessible, the proposed control system, composed of the Equation (19) and the allocation algorithm, was developed using the *C++* language and the input-commanding algorithm was deployed with *Python*. The block diagram of the implementation is presented in Figure 2, where the interaction between the algorithms can be appreciated, as well as the input and output signals from the *Gazebo*–ROS simulation system. In addition, the gains used for the proposed controller are listed in Table 1 and the parameters of the UAV for computing the allocator Equation (36) are presented in Table 2.

Below, the experiments to assess the control system performance are described, all of them working within the presented simulation framework.

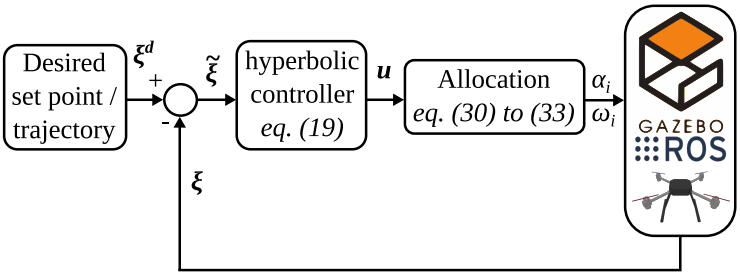

Figure 2. Block diagram of the closed-loop system.

Table 1. Gains of the proposed controller.

Gains	Value
$\mathbf{K}_p$	$\text{diag}(5, 5, 200, 10, 10, 10)$
$\mathbf{K}_i$	$\text{diag}(4, 4, 100, 2, 2, 2)$
$\mathbf{K}_v$	$\text{diag}(0.1, 0.1, 50, 0.3, 0.3, 0.3)$

Table 2. Parameters of the allocation matrix.

Parameter	Value
l	0.183847763
k_f	8.54858×10^{-5}
k_τ	$1.75\text{e}\times10^{-4}$

5.2. Tracking

The first experiment consisted of commanding the actively tilting quadrotor to perform the following trajectory for 100 s

$$\begin{cases} {}^W x_b^d &= \sin(3at)\cos(at)\ \text{m}, \\ {}^W y_b^d &= \sin(3at)\sin(at)\ \text{m}, \\ {}^W z_b^d &= 1 + bt\ \text{m}. \end{cases} \tag{41}$$

where $0 \leq t \leq 100$ is the time, $a = 0.075$ and $b = 0.025$. It was also desired that all the orientation angles remained at zero, but beforehand, the UAV should take off from $\mathbf{p}_b = (0, 0, 0)$ m to $\mathbf{p}_b^d = (0, 0, 1)$ m, with a zero orientation as well, in order to demonstrate that the translational motion is carried out by the tilting propellers rather than generated by the *roll* and *pitch* angles as in the case of nontilting quadrotors. Ten seconds after the

take-off, the UAV must track the given trajectory Equation (41) for 100 s as mentioned before. The first and second time derivatives of Equation (41) were obtained numerically.

Figure 3 shows the error norms of both position and orientation of the airframe with respect to the world frame. The 0.8 m peak at the beginning corresponds to the take-off, and up to second 10, the UAV remains hovering. Then, the tracking task starts after second 10 and it lasts until second 110; in such a period, the position error norm does not exceed 0.05 m, and it converges to zero afterwards until the end of the experiment. In addition, the orientation error does not reach 0.08 deg during the tracking, and it converges to zero at the end of the task as well.

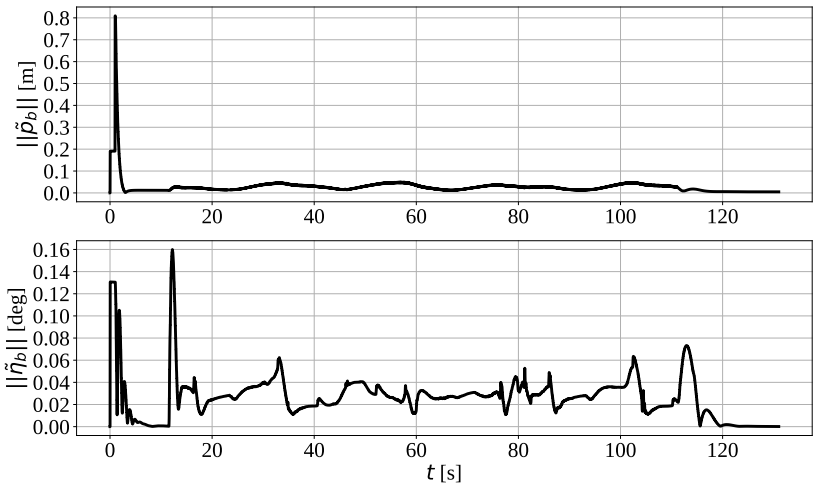

Figure 3. Error norms while the actively tilting quadrotor tracks the given trajectory. Top: position error. Bottom: orientation error.

The Cartesian motion of the UAV is displayed in Figure 4. The left part shows the top view of the trajectory, whereas the right part is a projected view of the performed Cartesian motion. It can be observed in both aforesaid figures that the desired trajectory is tracked with a slight mismatch, which is consistent with the position error norm exhibited in Figure 3. From the authors' perspective, the position tracking error average of 0.018 m represents an acceptable performance for the proposed control system.

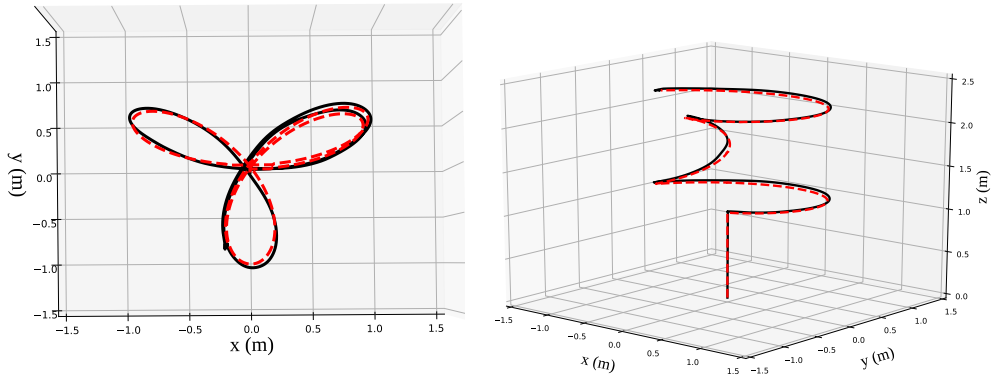

Figure 4. Performed trajectory in Cartesian space. Left: top view. Right: projected view. - - - Desired trajectory. — Performed trajectory.

5.3. Regulation Towards Far Set Points

In order to prove the global attractiveness provided by the proposed controller, the UAV was commanded to reach significantly far set points without giving any smooth trajectory between them, namely, the points were given as step inputs. Such points were

$$\begin{cases} \mathbf{p}_{b1}^{d} &= (0,0,2)\text{ m}, \\ \mathbf{p}_{b2}^{d} &= (5,5,3)\text{ m}, \\ \mathbf{p}_{b3}^{d} &= (5,0,3)\text{ m}, \\ \mathbf{p}_{b4}^{d} &= (0,5,3)\text{ m}. \end{cases} \tag{42}$$

Figure 5 shows the time evolution of the position and orientation errors of the performed experiment. The 2 m peak in the position error norm at 5 s corresponds to the point $\mathbf{p}_{b1}^{d}$, which is the commanded take off. The peak slightly larger than 7 m at 15 s corresponds to the norm of the commanded point $\mathbf{p}_{b2}^{d}$. Similarly, the third and fourth peaks denote the norms of the points $\mathbf{p}_{b3}^{d}$ and $\mathbf{p}_{b4}^{d}$, respectively. Notice that in all the cases, the norm converged to zero, despite an overshoot of 0.25 m for the case of large distances. With respect to the orientation norm, after the change of references, it converged to zero and remained steady before the position norm did, notwithstanding the overshoots.

Figure 6 displays the Cartesian motion plots of the actively tilting quadrotor during the experiment. In the top view, it can be appreciated that the UAV was not following a trajectory, but instead it flew directly to the commanded points. Moreover, the projected view is helpful to appreciate the same behaviour for the case of the vertical motion.

The results of this experiment confirmed that the ball $\mathbf{B}_r$ was globally attractive, because the trajectories of the error always converged to zero no matter how far they were the from the origin, which was also the centre of $\mathbf{B}_r$. This result is remarkable for a model-free controller, since other controllers from the literature require smooth input trajectories to work properly. Instead, the proposed controller will achieve any point $\mathbf{p}_{b}^{d}$, notwithstanding how far it is, and without planning a trajectory to achieve such a point.

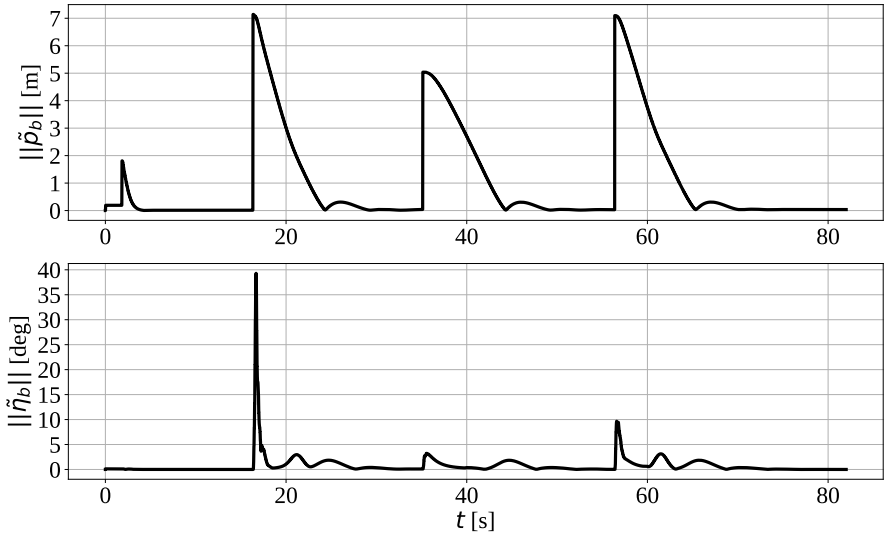

Figure 5. Position and orientation error norms while achieving set points far away from the current position. Top: position error norm. Bottom: orientation error norm.

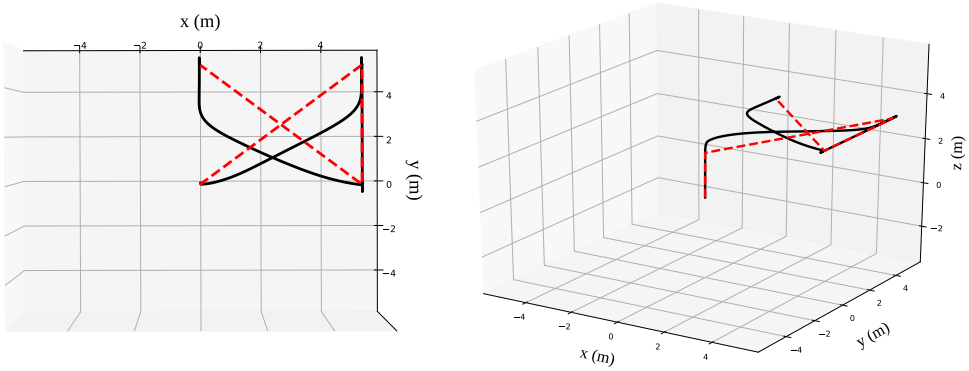

Figure 6. Performed trajectory in Cartesian space given a set of far set points. Left: top view. Right: projected view. - - - Distances between the desired points. — Performed trajectory.

5.4. Robustness Against Disturbances

Robustness is an important feature that a novel controller must offer. It is well known that UAVs might be affected by external disturbances, such as wind gusts, while flying outdoors; nonetheless, such a scenario is less probable in indoor environments. For such a reason, a different type of disturbance is proposed to test the robustness of the controller in study. A three-DOF serial robotic arm was attached to the actively tilting quadrotor, turning it into an aerial manipulator.

Figure 7 describes the new system and its coordinate frames. As it was mentioned before, the manipulator on board had three DOFs, namely, its rotational joints q_1, q_2 and q_3, as depicted in the figure. Since each joint of the manipulator was already controlled in position, then the Cartesian position of the end-effector frame with respect to the airframe could be easily controlled by means of the inverse kinematics of the arm. Now, from the dynamics point of view, the motion of the manipulator provided a coupling wrench that affected the UAV while flying, which might cause deviations in its position and orientation [20].

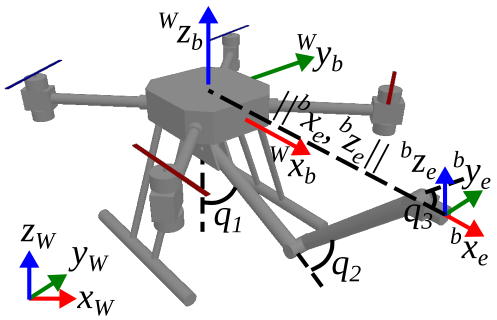

Figure 7. Actively tilting quadrotor with a robotic manipulator on board.

In this context, a useful benchmark was proposed in [20], which consisted of commanding the UAV to a certain position and, afterwards, the manipulator was directed to perform determined motions while the UAV tried to remain in a fixed position. The proposed metrics consisted of the maximum of the position error norm $\|\tilde{\mathbf{p}}_b\|$ and the elapsed time until $\|\tilde{\mathbf{p}}_b\| < 0.1L$ [20], where L was the reach of the manipulator, in this case $L \triangleq \max \|{}^b x_e, {}^b z_e\| = 0.46$ m.

The experiment consisted of commanding the UAV to take off and, after almost 20 s, start moving the end effector of the arm to the following points with respect to the airframe

$$\begin{cases} \begin{pmatrix} {}^b x_{e\,1}^d, & {}^b z_{e\,1}^d \end{pmatrix} & = & (0.25, 0) & \text{m}, \\ \begin{pmatrix} {}^b x_{e\,2}^d, & {}^b z_{e\,2}^d \end{pmatrix} & = & (0.35, 0.03) & \text{m}, \\ \begin{pmatrix} {}^b x_{e\,3}^d, & {}^b z_{e\,3}^d \end{pmatrix} & = & (0.25, -0.2) & \text{m}, \\ \begin{pmatrix} {}^b x_{e\,4}^d, & {}^b z_{e\,4}^d \end{pmatrix} & = & (0.35, 0) & \text{m}. \end{cases} \tag{43}$$

Figure 8 illustrates the joint positions and the end effector norm as well. It can be seen that the variations of the end-effector distances were significantly large, which could be also deduced from the motion of the joints. Moreover, Figure 9 presents the time evolution of the position and orientation errors norms of the UAV, which was almost 20 s longer since the manipulation motion started later. It can be noticed that $\|\tilde{\mathbf{p}}_b\|$ was always less than 0.02 m while the robotic arm was moving; therefore, according to the benchmark metrics $0.02 < 0.1L$, it proved that the proposed controller was robust enough to overcome the coupling wrench incoming from the manipulator.

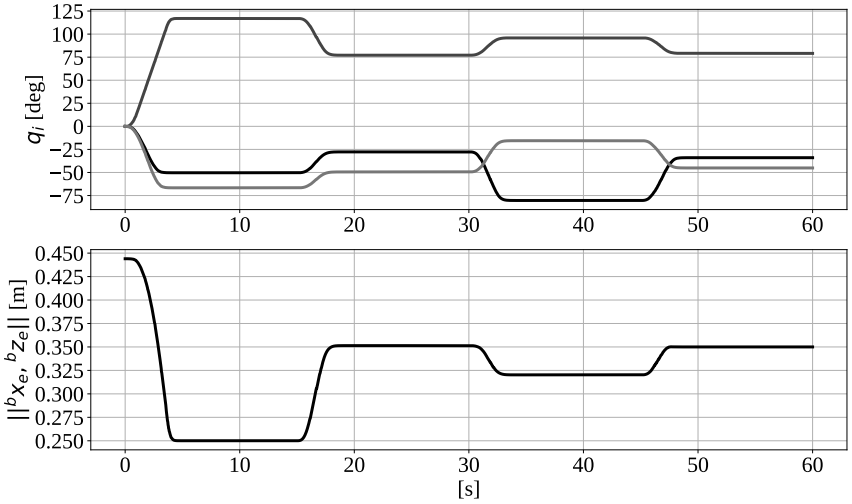

Figure 8. Motion of the on board manipulator. Top: joint positions. — q_1. — q_2. — q_3. Bottom: end effector's Cartesian motion norm.

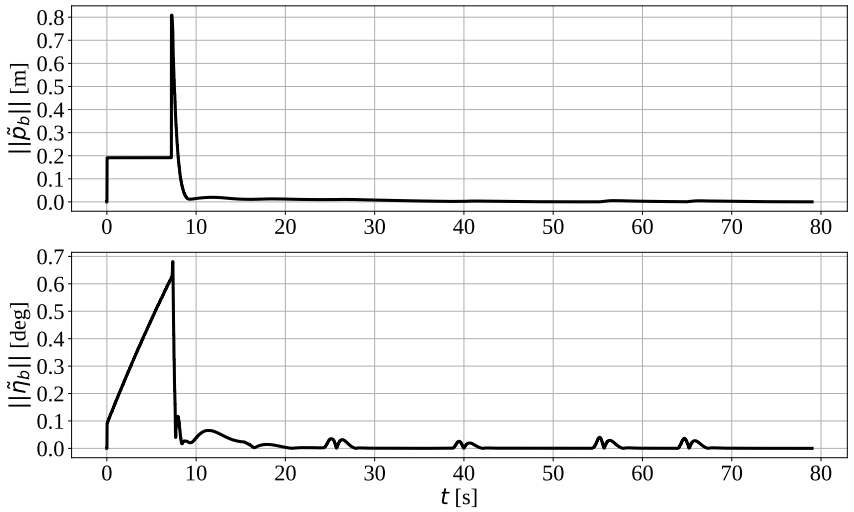

Figure 9. Time evolution of the position and orientation error norms of the UAV while moving the onboard manipulator. Top: position error norm. Bottom: orientation error norm.

5.5. Comparative Study

The final assessment was a comparison of the proposed controller against a state-of-the art technique. The contrasted controller was a nonlinear PID scheme almost identical to the one presented in [21], but with some slight modifications to work on the actively tilting quadrotor and which was given by

$$\begin{aligned}\mathbf{u} = \quad & \boldsymbol{\Gamma}(\boldsymbol{\eta}_b)^{-1}\Bigg[\mathbf{K}_p\tilde{\boldsymbol{\xi}} + \mathbf{K}_i\mathbf{sat}_{\gamma_0}\left(\int_0^t \dot{\tilde{\boldsymbol{\xi}}}(\vartheta) + c_1\tilde{\boldsymbol{\xi}}(\vartheta)\, d\vartheta\right) + \mathbf{K}_v\dot{\tilde{\boldsymbol{\xi}}} + \\ & mg\begin{bmatrix}\mathbf{e}_3\\ \mathbf{0}_3\end{bmatrix} + \mathbf{D}(\boldsymbol{\xi})\ddot{\boldsymbol{\xi}}^d\Bigg],\end{aligned} \tag{44}$$

where $\mathbf{sat}_{\gamma_0}(\cdot) : \mathbb{R}^6 \to \mathbb{R}^6$ is a componentwise saturation function with limit $\gamma_0 > 0$ and ϑ is an integration time interval. Since Equation (44) is model-based, the parameters were also obtained from the URDF model and are listed in Table 3. Furthermore, the gain matrices were the same as those used for the proposed controller appearing in Table 1. The comparison consisted of commanding some desired points to the UAV within an interval of 20 s in the middle of each one, and without planning any smooth trajectory between them. The same experiment was carried out for both controllers, and the target set points were the following

$$\begin{cases} \mathbf{p}_{b1}^d &= (0, 0, 1)\text{ m}, \\ \mathbf{p}_{b2}^d &= (0.5, 0.5, 1.5)\text{ m}, \\ \mathbf{p}_{b3}^d &= (0, 5, 2.5)\text{ m}. \end{cases} \tag{45}$$

Table 3. Parameters of the actively tilting quadrotor dynamics.

Parameter	Value
m	5 kg
$\mathbf{J}_b$	$\text{diag}(0.1522, 0.1522, 0.1841)$ kg m^2
g	9.81 m/s^2

Figure 10 shows the position and orientation error norms for both controllers. It can be noticed that the proposed controller settled the error signals up to eight seconds before than the nonlinear PID, also yielding less oscillations in both position and orientation norms. Additionally, the nonlinear PID caused larger orientation deviations than the hyperbolic controller. The performance was better until then using the hyperbolic controller; however, it was worth also analysing the control signals to have a better understanding of such results. Figure 11 shows the control signals resulting from the experiments of contrasting the aforementioned controllers. It can be seen that, for the same task, the rotors demanded more speed using the nonlinear PID controller, namely up to 2000 rpm more, whereas the tilting angles of the propellers changed at a lower frequency with the proposed hyperbolic technique. These results could be translated into obtaining a significantly better performance with up to one third of the energy consumption using the hyperbolic controller.

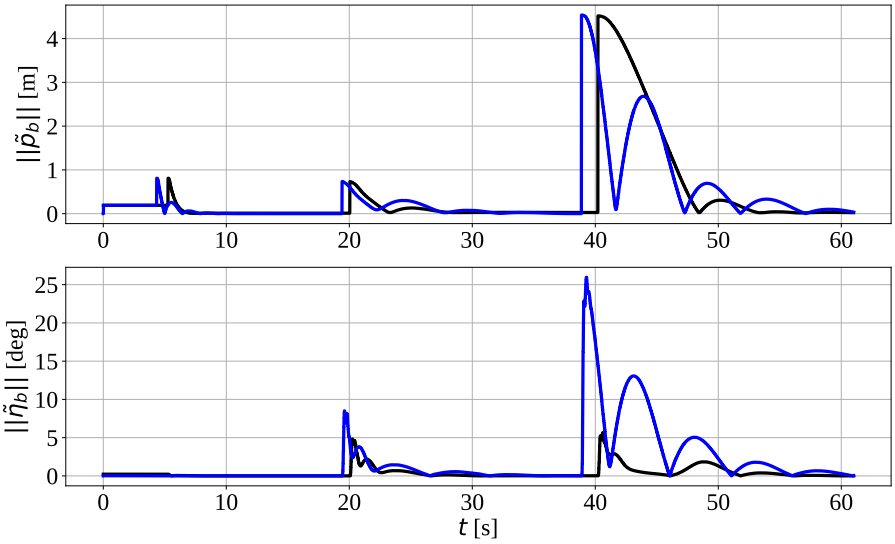

Figure 10. Position and orientation error norms while achieving the commanded set points. Top: position error norm. Bottom: orientation error norm. — Hyperbolic controller. — nonlinear PID controller.

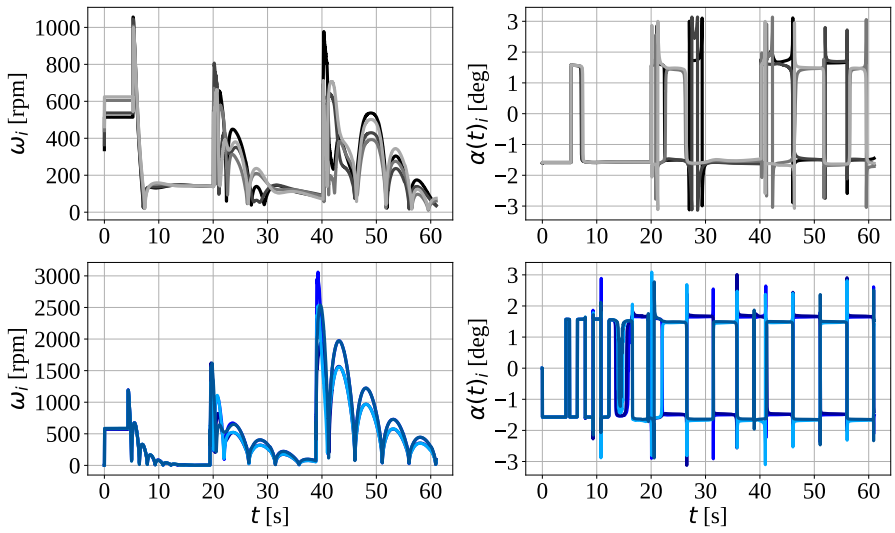

Figure 11. Control signals. Top Left: angular speeds of the rotors using the hyperbolic controller. Top right: Tilting angle of the propellers using the hyperbolic controller. — ω_1. — ω_2. — ω_3. — ω_4. Bottom Left: angular speeds of the rotors using the nonlinear PID controller. Bottom right: Tilting angle of the propellers using the nonlinear PID controller. — ω_1. — ω_2. — ω_3. — ω_4.

6. Conclusions

In this work, a hyperbolic control system for the robust flight of an actively tilting quadrotor was reported. The solution of the differential equations describing the closed-loop system, consisting of the UAV and the proposed controller, was analysed using a strict Lyapunov function. Through this analysis, it was demonstrated that the solutions were globally attracted to a small vicinity about the origin of the error signals space, which translated to an adequate tracking of the set points or trajectories in a physical sense.

Moreover, the effectiveness of the proposed hyperbolic control was evaluated through four different flight experiments performed in a physics-engine-based simulator, whose performance is almost identical to an actual experiment with a real UAV. The trajectory tracking experiment showed that the position errors norm never exceeded 0.05 m, which was an acceptable result due to the complexity of the trajectory.

The experiment consisting of commanding far set points reinforced the theoretical support of the global attractiveness of the controller, since the error signals always con-

verged to zero after changing abruptly the commanded set point, despite how far they were. Furthermore, the robustness evaluation, consisting in hovering steadily despite the motion of a coupled robotic arm, was also successfully fulfilled according to a benchmark from the literature.

A comparison of the hyperbolic controller against a state-of-the-art technique showed better performance and less energy consumption in favour of the former one. The hyperbolic controller settled the errors to zero up to eight seconds before and it demanded up to 2000 less rpm than the nonlinear PID to perform the same tasks.

The aforesaid successful results suggest that the proposed hyperbolic controller is an adequate alternative to effectively fly actively tilting quadcopters because of its simplicity, robustness, performance and low energy consumption. Thus, the readers of this manuscript are encouraged to implement the presented control approach in virtual or actual actively tilting quadrotors.

Author Contributions: Conceptualisation, S.M.O.S.; methodology, S.M.O.S.; software, S.M.O.S.; validation, S.M.O.S.; formal analysis, S.M.O.S. and F.R.; investigation, S.M.O.S.; resources, V.L.; data curation, S.M.O.S.; writing—original draft preparation, S.O; writing—review and editing, S.M.O.S., F.R. and V.L.; visualisation, S.M.O.S.; supervision, F.R. and V.L.; project administration, V.L.; funding acquisition, F.R. and V.L. All authors have read and agreed to the published version of the manuscript.

Funding: The research leading to these results has been supported by the AERIAL-CORE project (Horizon 2020 Grant Agreement No. 871479). The authors are solely responsible for its content.

Institutional Review Board Statement: Not applicable.

Informed Consent Statement: Not applicable.

Data Availability Statement: Not applicable.

Conflicts of Interest: The authors declare no conflict of interest.

References

1. Rashad, R.; Goerres, J.; Aarts, R.; Engelen, J.B.; Stramigioli, S. Fully actuated multirotor UAVs: A literature review. *IEEE Robot. Autom. Mag.* **2020**, *27*, 97–107. [CrossRef]
2. Papachristos, C.; Alexis, K.; Tzes, A. Efficient force exertion for aerial robotic manipulation: Exploiting the thrust-vectoring authority of a tri-tiltrotor uav. In Proceedings of the 2014 IEEE International Conference on Robotics and Automation (ICRA), Hong Kong, China, 31 May–7 June 2014; pp. 4500–4505.
3. Reyes-Cortes, F.; Felix-Beltran, O.; Cid-Monjaraz, J.; Alonso-Aruffo, G. A family of hyperbolic-type control schemes for robot manipulators. *Kybernetika* **2019**, *55*, 561–585. [CrossRef]
4. Nemati, A.; Kumar, M. Non-linear control of tilting-quadcopter using feedback linearization based motion control. In Proceedings of the Dynamic Systems and Control Conference, San Antonio, TX, USA, 22–24 October 2014; Volume 46209, p. V003T48A005.
5. Kumar, R.; Nemati, A.; Kumar, M.; Sharma, R.; Cohen, K.; Cazaurang, F. Tilting-rotor quadcopter for aggressive flight maneuvers using differential flatness based flight controller. In Proceedings of the Dynamic Systems and Control Conference, Tysons Corner, VA, USA, 11–13 October 2017; Volume 58295, p. V003T39A006.
6. Kumar, R.; Bhargavapuri, M.; Deshpande, A.M.; Sridhar, S.; Cohen, K.; Kumar, M. Quaternion feedback based autonomous control of a quadcopter uav with thrust vectoring rotors. In Proceedings of the 2020 American Control Conference (ACC), Denver, CO, USA, 1–3 July 2020; pp. 3828–3833.
7. Ryll, M.; Bülthoff, H.H.; Giordano, P.R. A novel overactuated quadrotor unmanned aerial vehicle: Modeling, control, and experimental validation. *IEEE Trans. Control Syst. Technol.* **2014**, *23*, 540–556. [CrossRef]
8. Invernizzi, D.; Giurato, M.; Gattazzo, P.; Lovera, M. Full pose tracking for a tilt-arm quadrotor UAV. In Proceedings of the 2018 IEEE Conference on Control Technology and Applications (CCTA), Copenhagen, Denmark, 21–24 August 2018; pp. 159–164.
9. Offermann, A.; Castillo, P.; De Miras, J. Nonlinear model and control validation of a tilting quadcopter. In Proceedings of the 2020 28th Mediterranean Conference on Control and Automation (MED), Saint-Raphaël, France, 15–18 September 2020; pp. 50–55.
10. Alkamachi, A.; Ercelebi, E. H∞ control of an overactuated tilt rotors quadcopter. *J. Cent. South Univ.* **2018**, *25*, 586–599. [CrossRef]
11. Wang, Z.; Li, J.; Duan, D. Manipulation strategy of tilt quad rotor based on active disturbance rejection control. *Proc. Inst. Mech. Eng. Part G J. Aerosp. Eng.* **2020**, *234*, 573–584. [CrossRef]
12. Ji, R.; Li, D.; Ma, J. Adaptive Second-Order Fast Nonsingular Terminal Sliding Mode Control for a Tilting Quadcopter. In Proceedings of the 2022 13th Asian Control Conference (ASCC), Jeju, Korea, 4–7 May 2022; pp. 403–408.
13. Sridhar, S.; Kumar, R.; Radmanesh, M.; Kumar, M. Non-linear sliding mode control of a tilting-rotor quadcopter. In Proceedings of the Dynamic Systems and Control Conference, Tysons Corner, VA, USA, 11–13 October 2017; Volume 58271, p. V001T09A007.

14. Nikhilraj, A.; Simha, H.; Priyadarshan, H. Modeling and Control of port dynamics of a tilt-rotor quadcopter. *IFAC-PapersOnLine* **2022**, *55*, 746–751. [CrossRef]
15. Ji, R.; Ma, J.; Ge, S.S.; Ji, R. Adaptive second-order sliding mode control for a tilting quadcopter with input saturations. *IFAC-PapersOnLine* **2020**, *53*, 3910–3915. [CrossRef]
16. Lu, K.; Yang, Z.; Liao, L.; Jiang, Y.; Xu, C.; Xu, H.; Zhang, Q. Extended state observer-based robust control of an omnidirectional quadrotor with tiltable rotors. *Trans. Inst. Meas. Control* **2021**, *43*, 1143–1155. [CrossRef]
17. Ruggiero, F.; Cacace, J.; Sadeghian, H.; Lippiello, V. Passivity-based control of VToL UAVs with a momentum-based estimator of external wrench and unmodeled dynamics. *Robot. Auton. Syst.* **2015**, *72*, 139–151. [CrossRef]
18. Santibáñez, V.; Kelly, R. Strict Lyapunov functions for control of robot manipulators. *Automatica* **1997**, *33*, 675–682. [CrossRef]
19. Rajappa, S.; Ryll, M.; Bülthoff, H.H.; Franchi, A. Modeling, control and design optimization for a fully-actuated hexarotor aerial vehicle with tilted propellers. In Proceedings of the 2015 IEEE international conference on robotics and automation (ICRA), Seattle, WA, USA, 26–30 May 2015; pp. 4006–4013.
20. Suarez, A.; Vega, V.M.; Fernandez, M.; Heredia, G.; Ollero, A. Benchmarks for aerial manipulation. *IEEE Robot. Autom. Lett.* **2020**, *5*, 2650–2657. [CrossRef]
21. Goodarzi, F.; Lee, D.; Lee, T. Geometric nonlinear PID control of a quadrotor UAV on SE (3). In Proceedings of the 2013 European Control Conference (ECC), Zurich, Switzerland, 17–19 July 2013; pp. 3845–3850.